LAWRENCE
LIVERMORE
NATIONAL
LABORATORY

UCRL-JRNL-225225

High-Resolution Adaptive Optics Scanning Laser Ophthalmoscope with Dual Deformable Mirrors

D. C. Chen, S. M. Jones, D. A. Silva, S. S. Olivier

October 11, 2006

Journal of Optical Society of America, A

High-Resolution Adaptive Optics Scanning Laser Ophthalmoscope with Dual Deformable Mirrors

Diana C. Chen, Steven M. Jones, Dennis A. Silva, Scot S. Olivier

Lawrence Livermore National Laboratory

6000 East Avenue, Livermore, CA 94539

Abstract: Adaptive optics scanning laser ophthalmoscope (AO SLO) has demonstrated superior optical quality of non-invasive view of the living retina, but with limited capability of aberration compensation. In this paper, we demonstrate that the use of dual deformable mirrors can effectively compensate large aberrations in the human retina. We used a bimorph mirror to correct large-stroke, low-order aberrations and a MEMS mirror to correct low-stroke, high-order aberration. The measured ocular RMS wavefront error of a test subject was 240 nm without AO compensation. We were able to reduce the RMS wavefront error to 90 nm in clinical settings using one deformable mirror for the phase compensation and further reduced the wavefront error to 48 nm using two deformable mirrors. Compared with that of a single-deformable-mirror SLO system, dual AO SLO offers much improved dynamic range and better correction of the wavefront aberrations. The use of large-stroke deformable mirrors provided the system with the capability of axial sectioning different layers of the retina. We have achieved diffraction-limited *in-vivo* retinal images of targeted retinal layers such as photoreceptor layer, blood vessel layer and nerve fiber layers with the combined phase compensation of the two deformable mirrors in the AOSLO.

OCIS: 170.1790, 170.3890, 170.4470, 230.3990, 330.4460

INTRODUCTION

The invention of confocal scanning laser ophthalmoscope (SLO) [1-2] has brought significant advances in real-time retinal imaging quality in terms of improved imaging resolution and increased light collection efficiency. The use of adaptive optics in the scanning laser ophthalmoscope (AOSLO) [3-5] to correct ocular aberrations of human retina has further increased the imaging quality by reducing the wavefront errors in both illumination and detection optical paths and achieved unprecedented optical quality.

The ocular aberrations of the test subjects are measured by a wavefront sensor in the AOSLO system. The measured wavefront errors are used to shape the adaptive optics (AO) or the deformable mirror (DM) until the wavefront entering the image detector has no residual aberrations. High resolution, diffraction-limited images are thus acquired. DMs are the key components in the realization of the practical and effective AOSLO system. Many deformable mirrors technologies such as mechanical mirrors with piezoelectric actuators, liquid crystal spatial light modulators, micro-electro-mechanical-system (MEMS) deformable mirrors, etc. [6-9] have been investigated for active phase compensation. Mechanical DMs are typically bulky and expensive, and not scalable to large number of actuators. Liquid crystal spatial light modulators have the issue of accurate phase controls. Existing MEMS technology provides limited amount of strokes.

If the test subjects have large-stroke, high-order aberrations, current DM technology cannot deliver the phase compensation needed using a single DM in a compact AOSLO system. To address the issue, we propose to use the multiple deformable mirrors in the AOSLO. Particularly, we employed the first DM to correct large-stroke, low-order aberrations and the second DM to correct low-stroke, high-order aberrations. Collectively, the dual deformable mirrors provided the necessary real-time ocular aberration corrections so that diffraction-limited *in-vivo* retinal images are achieved.

In this paper, we will discuss the development and image results of the dual-deformable mirror adaptive optics scanning laser ophthalmoscope system.

METHODS

Optical System

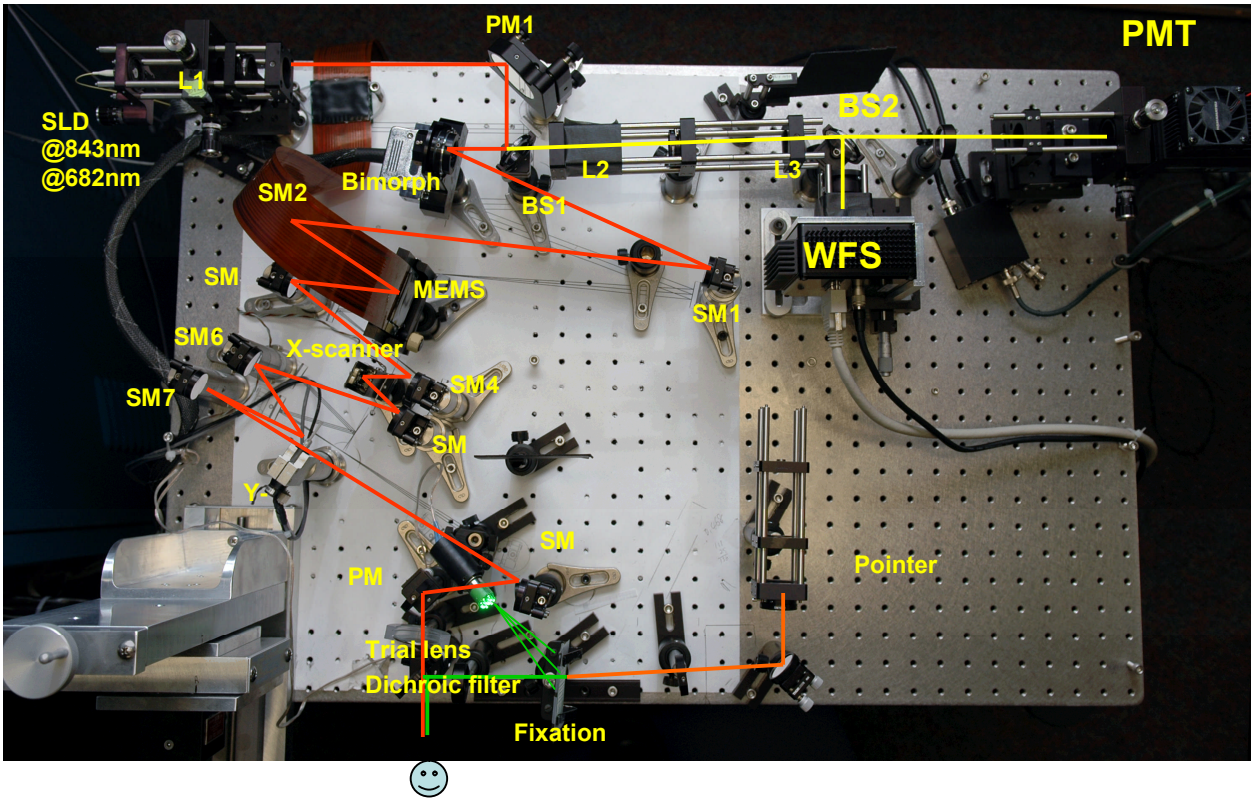

Fig.1. Top view of the dual DM adaptive optics scanning laser ophthalmoscope system. SLD, Superluminescent Laser Diode; L, lens; BS, Beam splitter; PM, Plane Mirror: SM, Spherical Mirror; WFS, Wavefront Sensor; PMT, Photomultiplier Tube

The dual-DM AOSLO system is developed for clinical study at Doheny Eye Research Center. The key goals for the optical system design are (1) high resolution imaging (2) effective ocular aberration correction (3) compact, portable assembly for clinical environment. Figure 1 shows the top view of the dual-deformable-mirrors adaptive optics scanning laser ophthalmoscope system. The optical system consists of several key function groups – light delivery, wavefront sensing, wavefront compensation, scanning optics and image detection.

Ocular aberration correction is achieved by placing the Shack-Hartmann wavefront sensor and the two DMs at the phase conjugated planes of the eye pupil. Each component is placed at the focal plane of the relay afocal telescopes. To reduce back reflection, spherical mirrors, instead of lenses, are used in the afocal telescope design. This brings the additional benefit of minimal chromatic aberrations when light source of wide bandwidth or different wavelength is used. One of the issues using the reflective mirrors is the off-axis configuration would introduce astigmatism. This problem is solved by optimizing the system design and adding a cylindrical compensation lens in the AOSLO.

Horizontal and vertical scanners are placed at the phase conjugated planes of the eye pupil to ensure that no movement at the pivot point. The diffused reflected light from the retina travels inversely along the incoming illumination path to the two scanners, the two DMs and is relayed by a telescope, and finally separated by a pellicle beamsplitter to the wavefront sensor and photodetector. An optical aperture is placed at the focal point of the telescope to reduce the stray light in the AOSLO. A confocal pinhole is placed at the focal point of the collection lens. All the optical components are assembled to a 2'x3' optical breadboard with wheels so that the ophthalmoscope can be easily moved to different offices in an ophthalmology clinic (see Fig.2).

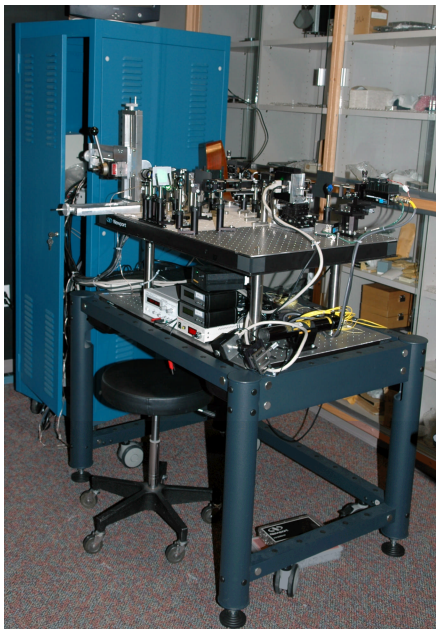

Fig. 2 Portable AOSLO system side view. Optical components are mounted on the top of 2'x3' rollable cart and all electronics are mounted onto the rack for mobility.

Light Delivery

Two light sources, superluminescent diodes (SLD) from Superlum SLD-371-HP2-DBUT-SM-PD (λ_0 = 843.3 nm, $\Delta\lambda$ = 48.3 nm, P=18 mW) and SLD-261-HP1-DIL-SM-PD (λ_0 = 682 nm, $\Delta\lambda$ = 9.6 nm, P= 5 mW) were used in the AOSLO. Both light sources are fiber coupled and a compact package of a FC single mode fiber connector, an x-y-z stage for adjusting collimation lens, an achromatic lens, and a system aperture delivers collimated light of the desired wavelength into the AOSLO. The use of different wavelengths is accomplished by switching the incoming optical fibers to the light delivery package.

Wavefront Sensing

Wavefront sensing and the detection paths in the AOSLO were designed to share the same light path to eliminates the non-common path errors. The wavefront error was measured with a Shack-Hartmann wavefront sensor consisting of a 20x20 lenslet array (Adaptive Optics Associates, 0500-30-S-A, 500 um pitch, 30 mm focal length) and a CCD camera (Dalsa 1M60 CCD

CameraLink) at its focal plane. The wavefront sensor measures displacements of the spots produced by the lenslet array from its reference position. The AO-computer reads the displacements and determined the wavefront errors in the optical paths [10-11].

Wavefront Compensation:

Two deformable mirrors were employed to provide the wavefront compensation in the AOSLO. Both deformable mirrors were placed at the planes conjugated to the entrance pupil of the eye and they are also phase-conjugated to each other and to the wavefront sensor. The AO-control computer drives the Shack-Hartmann wavefront sensor and both deformable mirrors.

A bimorph deformable mirror (Aoptix Technologies, Inc.) was used to correct large-stroke aberration. It consists of layers of ceramic lead Magnesium Niobate that is directly actuated by the electrodes bonded on the material. The deformable mirror has 35 actuators which can be divided into two groups – curvature actuators and slope actuators. For the 35 element mirror, actuators 1 to 19 are curvature actuators, which produce curvature proportional to the applied voltage in the wavefront. Actuators 20 to 35 are slope actuators, which produce a radical slope proportional to the applied voltages in the wavefront. Actuator 20 is a guard ring which ensures a clean separation between curvature and slope actuators. The largest displacement of the bimorph deformable mirror is 16 μm for a 10 mm aperture, which can which can compensate up to 32 μm in wavefront deflection. Because the stroke of the bimorph scales with the inverse square of the spatial frequency of the Zernike mode and the highest spatial frequency mode is 5 cycles/diameter, the bimorph mirror is best used to compensate the large-stoke, low-order ocular aberrations.

The residual high-order, small-stroke aberrations were corrected by the MEMS mirror (Boston Micromachine, Inc.). It consists of a continuous membrane and supported by underlying actuator array of 12 x 12 elements with a 300 μm/actuator. Unlike the bimorph deformable mirror, each actuator is individually addressable and cross-talk between actuators is minimal. The largest displacement is 1.5 μm over 3 mm x 3mm area, which can which can compensate up to 3μm in wavefront deflection.

Deformable mirrors should be carefully calibrated as optical "flats" before they are placed in the AOSLO system so that no additional aberration is introduced to the optical paths by the DMs. When no biased voltages are applied to the electrodes, the bimorph mirror has a natural curvature of 0.3 D due to the mechanical stress in the different layers of the mirror materials. The MEMS has an RMS error of 90 nm created by the non-uniformity in the manufacturing process. In the calibration set-up, a perfect collimated light source illuminated the DM and the wavefront error was measured by the Shack-Hartmann wavefront sensor. The DM under calibration was placed at the phase-conjugated plane of the lenslet array of the wavefront sensor. The measured wavefront was used to calculate the voltages applied to the actuators of the DM and the DM was conformed to the desired shape. The iteration continued until the wavefront aberration was minimized and the AO operation stabilized. The AO computer saved the stabilized voltages and the shape of the DM is referenced as "Flat", which is the best experimental optical flat we could achieve with the deformable mirrors.

The wavefront compensation in the AOSLO was accomplished by the two-step process. The AO system started with the both DM in the position of the reference "Flat". When a subject's eye is tested, the AO-computer read the measured the system wavefront aberration from the Shack-Hartmann wavefront sensor and calculated the applied voltages to the bimorph mirror in closed-loop control. The bimorph mirror was re-shaped to minimum the wavefront aberrations while the MEMS mirror is hold in the reference flat position. The AO control iteration and the bimorph mirror typically took several seconds to stabilize. The bimorph mirror was then held "static". The residual wavefront aberrations were measured by the Shack-Hartmann wavefront sensor. The MEMS deformable was reshaped to minimize the wavefront aberrations [12-15].

Scanning optics

The focused beam is scanned on the retina in a raster pattern with a horizontal scanner (Electro-Optics Products Corp., SC-30 resonate scanner, 14 kHz, 6°) and a vertical scanner (Cambridge Technology, 6220M40 galvanometric scanner, ±20°). The two scanners are separated by a relay telescope ensuring that they are phase conjugated to each other and to the entrance pupil of the eye. This minimized the movement of the scanning beam at the pupil. The optical design is optimized for the field of view up to 3° x 3° for a 6 mm circular eye pupil. The scanned image corresponds to 0.9 mm x 0.9 mm area on retina.

Both horizontal and vertical scanners produce image wobbling effects on the entrance pupil of the eye. If an object plane is at an angle to the principle axis of an optical system, its related image plane is formed at an angle to the principle axis**.** Fig. 3 shows the object and image planes of a 2:1 telescope. The blue planes show the object and image planes when they are perpendicular to the optical axis and the black planes show the positions when they are at a slanted angle.

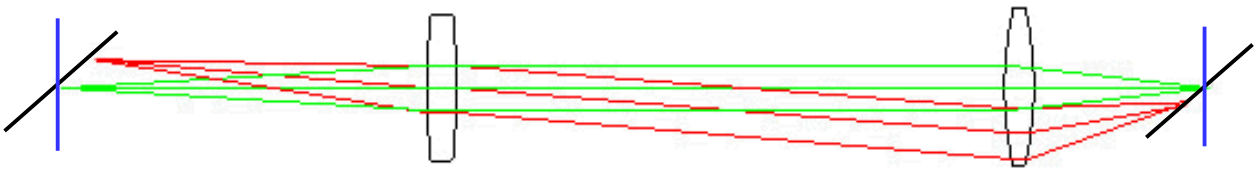

Fig. 3 shows that if an object plane is at an angle to the principle axis of an optical system, its related image plane is formed at an angle to the principle. The configuration is a 2:1 telescope. The blue planes show the object and image planes when they are perpendicular to the optical axis and the black planes show the positions when they are at a slanted angle.

From the simple illustration, we can tell that the optical phase conjugated plane of a scanner at the entrance pupil of the eye is not a fixed plane, but a rotating plane as a variable of the optical scanning angle. The projected optical spot size on the plane of the entrance pupil of the eye is thus a function of the scanning angle, producing an optical wobbling effect. Fig.4 show the spot sizes related to various scanning position (a) -1.5°, 0° , 1.5° horizontal scanning (b)- 1.5°, 0° , 1.5° horizontal scanning.

The wavefront measurement has no issue as long as the wobbling is small. The Shack-Hartmann wavefront sensor measured the average aberrations over the integration time and over the projected pupil of the eye. The combination of resonate scanner and galvanometric scanner provides raster images at 30 frame per second with 525 lines per frame. The Shack-Hartmann wavefront sensor consists of 20 x 20 lenslet arrays, with 2x2 lenslet arrays working as a function detection element. If the wobbling due to scanning is more than 1 lenslet when the wobbling is projected back to the pupil plane of the wavefront sensor, the wavefront sensor would not be able to correctly interpret the aberrations. The maximum wobbling allow in the current AOSLO is 300 µm to avoid wavefront registration errors.

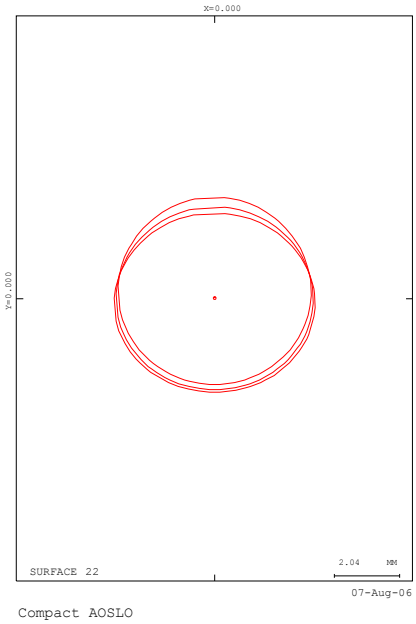

Fig. 4 (a)

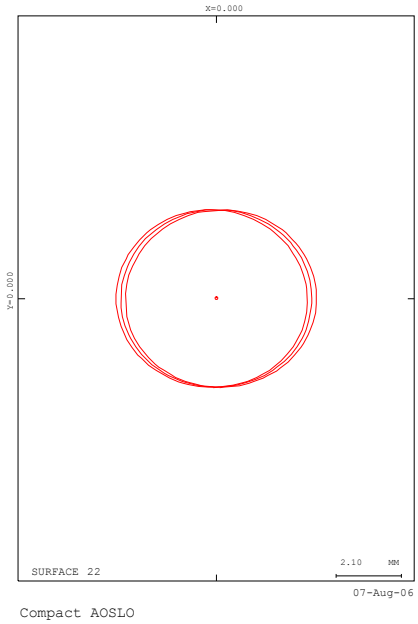

Fig. 4(b)

Fig.4 The spot sizes related to various scanning position (a) -1.5°, 0° , 1.5° horizontal scanning (b)- 1.5°, 0° , 1.5° horizontal scanning.

Image Detection:

After the wavefront compensation with deformable mirrors, the light coming from the retina finally focused through a confocal pinhole and detected with a GaAs photomultiplier tube (H7422-50, Hamamatsu). An achromatic lens with a 150 mm focal length was used to collect the light for the beam size of 10 mm in diameter. Axial resolution of the detected images increased with the decreased pinhole size, while the light throughput decreased with the decreased pinhole sizes [16-18]. A pinhole size of 100 µm was used in the current AOSLO and it was 1.5x diffraction-limited spot size at the confocal plane. The 100 µm pinhole provides the optimal compromise between the resolution and light throughput for the dual DM AOSLO system

The photons were detected by the PMT and the signal is fed to the frame grabbing board. The frame grabber presented the raw image of 500 x 500 pixels at 27 frames per second.

Subject test:

The subject was asked to view the fixation target to minimize head and eye motion and to allow precise imaging of different retinal locations. An image from the wavefront sensor was used to monitor the x-y position of the eye's pupil. A bite-bar assembly was mounted on an x-y-z translation stage on the optical table to permit precise positioning of the subject's eye. To ensure the maximum pupil size and minimize fluctuations in accommodation, the subject's eye was dilated and cyclopleged with 2.5% Phenylephrine and 1% Tropicamide for a 6 mm pupil.

The retinal image session started with the wavefront measurement, then closing loop with the bimorph mirror for the initial phase compensation. After the wavefront was stabilized, closing loop with the second deformable mirror MEMS to compensate the residual aberrations. Once the wavefront aberrations were minimized, the digital video recording started.

RESULTS

Imaging with and without AO correction

The dual-deformable-mirrors AOSLO is used in clinical settings to image both healthy and diseased eyes. Fig. 5 shows the retinal images acquired at the same area with/without aberration corrections using the dual deformable mirrors (a) without AO correction (b) First DM turned on (Bimorph) (c) Second DM turned on (MEMS). The images were taken with an 840 nm SLD. The imaging area was at the retinal location of 3° Nasal and 3° Superior and the field of view is 1.1°.

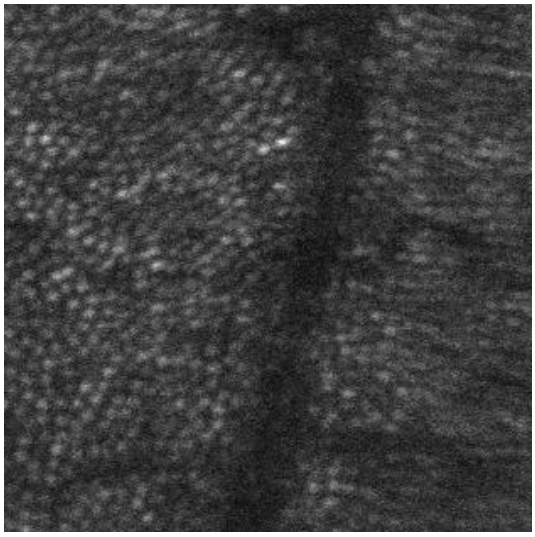

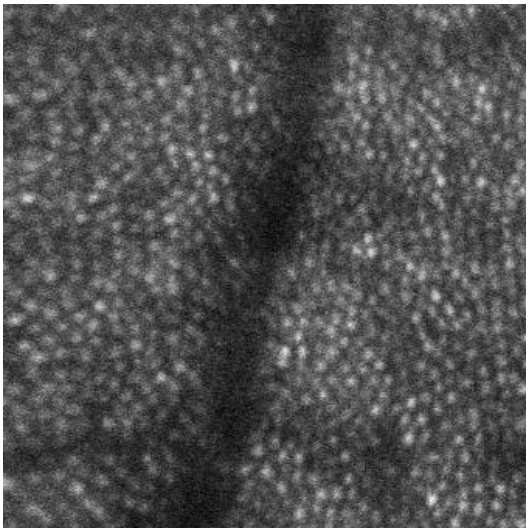

Fig5 (a) (b)

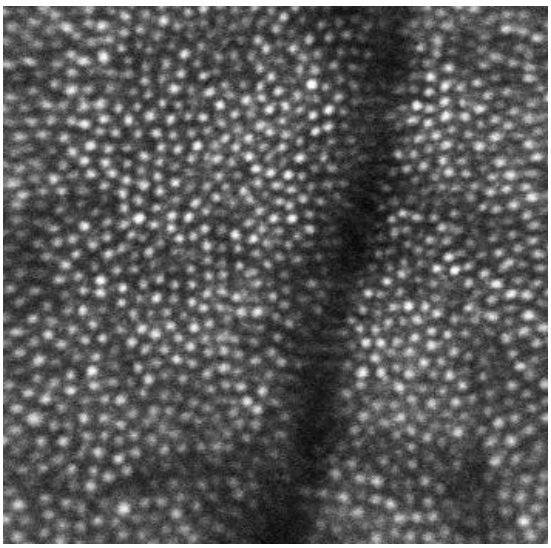

(c)

Fig. 5 Retina images with dual AO corrections taken at 3° Nasal/ 3° Superior Retina, 1.1° scanning angle at wavelength of 843 nm.(a) Without AO correction. (b) With closed-loop operation of the bimorph mirror (c) with closed-loop operation of the MEMS

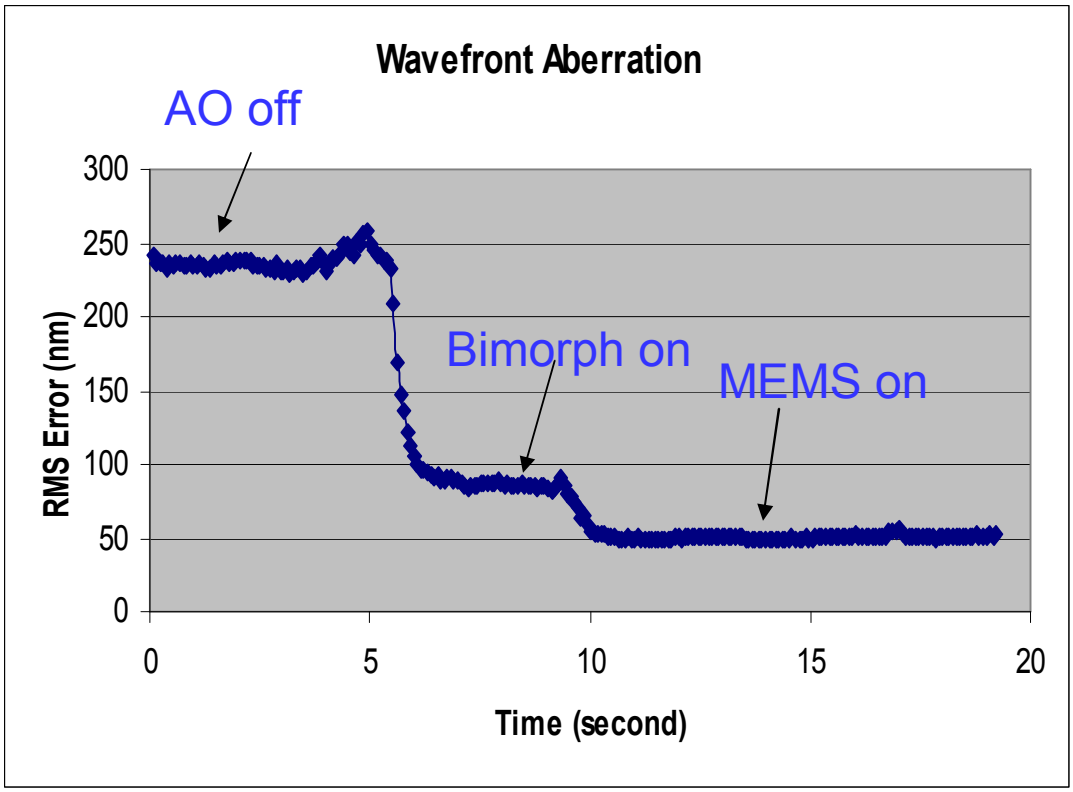

Fig. 6 Measured wavefront aberration over a 6 mm pupil before and after AO compensation

Fig. 6 shows the related RMS wavefront errors with and without the dual AOs. The RMS wavefront error without AO was 248 nm over 6 mm pupil, and it was reduced to 90 nm when the first deformable mirror was turned on. The MEMS further reduced RMS wavefront error to 48 nm. Strehl ratio is defined by the ratio of the intensity at the peak of the aberrated diffraction pattern to the intensity at the peak of an aberration-free image. The Strehl ratio was increased from 2% without AO correction to 55% with the first AO correction and 89% with the second AO correction. The AO corrected images showed higher resolution and increased brightness as the RMS wavefront error decreased with the AO correction.

Focus on targeted layers of retina

Fig. 7 shows the images acquired at the same area of the retina as in Fig. 5, when focusing on different layers of the retina. A difference matrix was added to the reference matrix when the AO computer calculated the voltages applied to the actuator. Optical curvatures were applied to the bimorph mirror so that targeted layers of retina are in focus. Fig. 7(a) shows the images of blood vessel layer and 7(b) shows the images of the nerve fiber layer while Fig. 5 shows the images of photoreceptor layer. Comparing three images, we can see that blood vessel appeared darker in Fig. 5. This is because the blood vessel layer was not in focus and the scattered light from its surface was blocked by the confocal pinhole when the photoreceptor layer was imaged. The total thickness of the retina is about 300 μm.

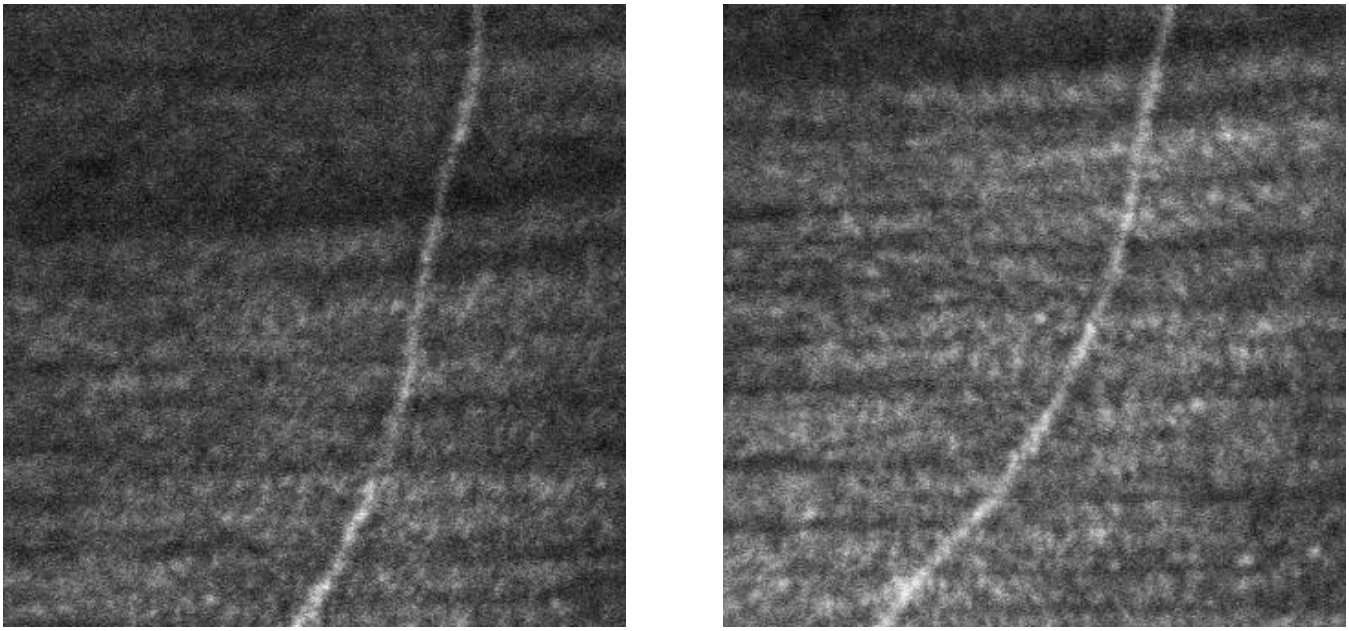

Fig 7(a) Blood vessel layer **(b) Nerve fiber layer**

Fig. 7 Retina images with dual AO corrections taken at 3° Nasal/ 3° Superior Retina, 1.1° scanning angle at wavelength of 843 nm.(a) Blood vessel layer (b) Nerve fiber layer

The movie file Fig. 8 shows the real-time image sequence when both DMs are applied to acquire high-resolution images of the nerve fiber layer. The movie started from the photoreceptor layer, and then the image is focused on the blood vessel layer by biasing the bimorph mirror. The blood cells can be clearly seen flowing through the vessel. Larger curvature is applied to the bimorph mirror, and the optical nerve fiber layer was in focus. Blood vessel layer and optical nerve fiber layer are close to the same optical plane, so they can be resolved at the same time in the movie. When the AO close-loop operation was stabilized with the bimorph mirror, MEMS was employed to further reduce the high-order aberrations. The images of optical nerve fiber became brighter with the second DM.

The dual DM AOSLO system provides the high-resolution imaging capability of any desired layers of retina. This multi-layer imaging capability can effectively save the clinicians time and efforts for retinal disease imaging and diagnosis in the clinical environment.

Large ocular aberration compensation without a trial lens

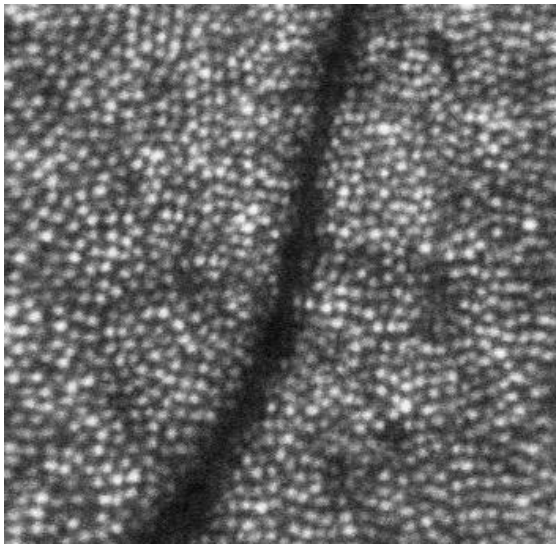

Fig. 9 Photoreceptor image of a test subject with -3D spherical aberration. The image was acquired with dual AO corrections at 3° Nasal/ 3° Superior Retina, 1.1° scanning angle at wavelength of 843 nm.

One of the major benefits of the dual deformable mirror AOSLO is that the bimorph mirror has a large deflection of 16 um which can compensate large ocular aberrations. Fig. 9 shows the movie of the photoreceptor layer of a subject with -3D spherical aberration. The movie was taken at the same area at the retina as in Fig. 5 using an 843 nm SLD. The spherical aberration was compensated with a trial lens in Fig. 5, while no trial lens was inserted in the AOSLO and all aberrations were compensated by the two deformable mirrors in Fig. 9. No retinal feature was detected by the AOSLO at the beginning without phase compensation. Then images of cones and blood vessel were observed with the compensation of the bimorph mirror. The images got substantially sharper and brighter with the additional phase compensation of the MEMS. The aberration-corrected photoreceptor image in Fig. 9 is of the similar quality compared to that of Fig. 5 (c)

This capability of large phase compensation can potentially eliminate the trial lens for many patients in the clinical environment. While more study needs to be done to carefully examine the limits of the instrument, the preliminary results show that the dual DM can compensate up to ± 3D spherical or ± 3D cylindrical aberrations.

CONCLUSIONS

We have demonstrated that multiple micro-deformable mirrors in an AOSLO system can effectively compensate both large, low-order and small, high-order aberrations in the human eye, and produce *in vivo* retinal images with nearly diffraction-limited resolution. Focusing through different layers of the retina is also made possible by the use of large-stroke micro-deformable mirrors and trial lenses could be potentially eliminated in clinical testing. Furthermore, the small size of the μDM's enables a compact optical design, making the AOSLO system a viable, portable, non-invasive, high-resolution imaging tool for clinical diagnostics.

ACKNOWLEDGEMENTS

This research was supported by the NIH grant EY014365 and performed under the auspices of the U.S. Department of Energy by University of California, Lawrence Livermore National Laboratory under Contract W-7405-Eng-48. All testing and imaging of subjects with this system was performed at the UC Davis Medical Center in collaboration with Stacey Choi, Robert Zawadzki and Jack Werner. We particularly benefited from technical discussions from Yuhua Zhang and Austin Roorda at UC Berkeley.

REFERENCES

1. R. Webb and G. Hughes, "Scanning laser ophthalmoscope," IEEE Trans. on Bio. Eng. **28**, 488-492 (1981)
2. R. Webb, G. Hughes, and F. Delori, "Confocal scanning laser ophthalmoscope,", Appl. Opt. **26**, 1492-1499 (1987)
3. J. Liang, D. Williams, and D. Miller, "Supernormal vision and high-resolution retinal imaging through adaptive optics", J/ Opt. Am. A **14**, 2884-2892 (1997).
4. A. Roorda, F. Romero-Borja, W. Donnelly, H. Queener, T. Herbert, and M. Campbell, "Adaptive optics scanning laser ophthalmoscopy", Opt. Exp. **10**. 405-412 (2002).
5. Y. Zhang, S. Poonja, and A. Roorda, "Adaptive optics scanning laser ophthalmoscope using a micro-electro-mechanical (MEMS) deformable mirror," Proc. of SPIE **6138** (2006)
6. H. Hofer, L. Chen, G. Yoon, B. Singer, Y. Yamauchi, and D. Williams, "Improvement in retinal image quality with dynamic correction of the eye's aberration," Optics Express, **8**, 631-643 (2001)
7. F. Vargas-Martin, P. Prieto, and P. Artal, "Correction of the aberrations in the human eye with a liquid-crystal spatial light modulator: limits to performance", J. Opt. Am. A **15,** 2552-2562 (1998).
8. T. Bifano, J. Perreault, P. Bierden, and C. Dimas, "Michromachined deformable mirrors for adaptive optics," Proc. of SPIE **4825**, 10-13 (2002)
9. N. Doble and D. Williams, "The applications of MEMS technology for adaptive optics in vision science," IEEE Quantum Electronics, **10**, 629-635 (2004)
10. G. Yoon, "Wavefront sensing and diagnostic users", 63-81, "Adaptive Optics for Vision Science", Wiley& Sons
11. J. Liang, B. Grimm, S. Goelz, J. Bille, "Objective measurement of wavefront aberrations of the human eye with the use of a Hartmann-Shack wave-front sensor," J. Opt. Am. A. **11**, 1949-1957, (1994)
12. S. Hu, B. Xu, X. Zhang, J. Hou, J. Wu and W. Jiang, "Double-deformable-mirror adaptive optics system for phase compensation", Appl. Opt. **45,** 2638-2642 (2006)
13. J. Barchers, "Closed-loop stable control of two deformable mirrors for compensation of amplitude and phase fluctuations," J. Opt. Am. A **19**, 926-945 (2002)
14. M. Roggemann and D. Lee, "Two-deformable-mirror concept for correcting scintillation efforts in laser beam projection through the turbulent atmosphere," J. Appl. Opt. **37**, 4577-4585 (1998)
15. M. Langlois, C. Saunter, C. Dunlop, R. Myers, and D. Love, "Multiconjugate adaptive optics: laboratory experience," Opt. Lett. **12**, 1689-1691 (2004)
16. Y. Zhang and A. Roorda, "Evaluating the lateral resolution of the adaptive optics scanning laser ophthalmoscope," J. of Bio. Opt. **11** (2006)
17. K. Venkateswaran, A. Roorda, and F. Romero-Borja, "Theoretical modeling and evaluation of the axial resolution of the adaptive optics scanning laser ophthalmoscope," J. of Bio. Opt. **9**, (2004)
18. Y. Zhang, S. Poonja, and A. Roorda, "MEMS-based adaptive optics scanning laser ophthalmoscope," Opt. Lett. **31**, 1268-1270 (2006)